Intraparticle Charge Delocalization through the Conjugated Metal-Ligand Interfacial Bonds: d-electrons Effect

Yi Peng, Eduardo Y. Hirata, Limei Chen, Jia-En Lu, Wanzhang Pan, Shaowei Chen*

Department of Chemistry and Biochemistry, University of California, Santa Cruz, 1156 High Street, Santa Cruz, CA, 95060, USA

Abstract

The intraparticle charge delocalization of conjugated ligand π electrons through the metal cores were systematically investigated in this study. 5d metals (Ir, Pt, and Au) and 4d metals (Ru, Rh, and Pd) were synthesized as the metal cores and ethynylphenylacetylene (EPA) was used as the model organic ligands that self-assembled on the surface of various metals. Both characteristic features of FTIR (the aromatic ring =C-H vibrational stretch peaks) and the photoluminescence indicates that the strength of intraparticle charge delocalization through the same period of d-metal cores is decreased with the increase of d-electrons, however, palladium is an exception.

Introduction

In the past decades, nanoparticles plays more and more important roles in a lot of areas and it has been recognized that the interfacial structure at the metal-ligands interfaces are significant and powerful parameter for the applications. Of which metal-thiolate (M-S),[1] metal-carboxylate (COOH-M), N-heterocyclic carbenes, and phosphines have been extensively investigated and been used in a plenty of areas such as photonics, drug deliveries, catalysts, electronics.[2-4] Recently, another kind of new interfacial structure of metal nanoparticles with conjugated ligands was explored in Chen group such as metal-carbon (including M-Ar, M=C, and M-C≡) and metal-nitrene (M=N).[5-9] Due to the efficient conjugation structure, there is strong intraparticle charge delocalization and thus a lot of interesting catalytic, optical and electronic properties were emerged.

In this kind of metal-conjugated ligand interfacial structures, two components should be taken into consideration, one is the organic conjugated ligand and the counterpart is metal nanoparticle core. In recently years, the ligand part has been widely studied for instance, Kang et al. claimed interfacial bonding structure on ruthenium nanoparticle should be Ru-vinylidene (Ru=C=CH-) rather than metal-acetylide (Ru-C≡) by a specific reactivity of the nanoparticle with imine derivatives.[10] Hu et al. further proved that the interfacial bonding structure on platinum nanoparticles should be in the equilibrium of Pt-C≡C-/Pt-H and Pt=C=CH- while Pt=C=CH- is the dominating structure by using isotopic labeled alkyne ligands.[11] As for the metal core counterparts, only several fragmentary works has been done. For example, it was found that the strength of intraparticle charge delocalization could be manipulated by the nanoparticle charge state.[12] Though several metal nanoparticles capped by conjugated ligands were successfully synthesized such as Cu, Ru, Pd, Pt, AuAg alloy and PdAu alloy,[13-19] there is no systematic investigation about how different metals affect the intraparticle charge delocalization through the interfacial bonding. This is the main motivation of the current study.

Herein, ethynylphenylacetylene was chosen as surface ligand and two sets of metals nanoparticles including 5d metals Ir, Pt and Au, and 4d metals Ru, Rh and Pd were successfully synthesized as metal cores. The morphology and size of these metal nanoparticles were first characterized by transition electronic microscopic (TEM) measurement. And the intraparticle charge delocalization through various metal cores was systematically investigated by comparing

their FTIR and photoluminescence. The results indicated that the strength of intraparticle delocalization of conjugated ligand π electrons through the metal cores in the same period were decreased with the increase of the number of d-electrons while palladium is an exception which is understandable as the electron affinity of the palladium doesn't obey the trend in the 4d metals.

Experimental Section

Chemicals. Ruthenium chloride ($RuCl_3$, Acros), Rhodium chloride ($RhCl_3$, Acros), Palladium chloride ($PdCl_2$, Acros), Iridium chloride ($IrCl_3$, Acros), Platinum chloride ($PtCl_4$, Acros), hydrogen tetrachloroauric acid ($HAuCl_4$, Sigma-Aldrich), 4-ethynylphenylacetylene (EPA, 97%, Acros). Solvents were purchased at the highest purity available from typical commercial sources and also used as received. Water was deionized with a Barnstead Nanopure Water System (18.3 MΩ·cm).

Synthesis of Ru, Rh, Ir and Pt nanoparticles. The synthesis of Ru, Rh, Ir and Pt nanoparticles were adopting the literature with some modification. Briefly, 0.3 mmol of metal chloride ($RuCl_3$, $RhCl_3$, $IrCl_3$, $PtCl_4$) were dissolved in 5 mL water and then was added into 100 mL ethylene glycol with strong stirring, and followed by adding 5 mL 0.5 M NaOH solution under nitrogen environment. After 20 min strong stirring, metal nanoparticles were produced by heating the homogeneous solution to 160 °C for 3 hours. After the product was cooled down to room temperature, 50 mL toluene and 0.9 mmol ethylphenylacetylene (EPA, keep the mol ratio of EPA to metal at 3:1) were added into the solution. After 12 hours ligand exchange at 60 °C under strong stirring, the nanoparticles were transferred into the toluene phase. The toluene phase was collected, dried by rotary evaporation, and rinsed extensively with methanol to obtained purified metal nanoparticles and were denoted as M-EPA (M=Ru, Rh, Ir, Pt).

Synthesis of Pd and Au nanoparticles. The synthesis of Au and Pd nanoparticles were adopting the literature with some modification. Briefly, 200 mg PVP was dissolved in 45 mL water and mixed with another 45 mL of 2 mM $HAuCl_4$ or $H2PdCl_4$ then the solution was kept in ice bath for 30 min, following by adding 5 mL NaBH4 solution (containing 35 mg NaBH4) with continuous strong stirring for 15 min. After the product was warmed up to room temperature, 45 mL toluene and 0.27 mmol ethylphenylacetylene (EPA, keep the mol ratio of EPA to metal at 3:1) were added into the solution. After 12 hours ligand exchange at 60 °C under strong stirring, the nanoparticles were transferred into the toluene phase. The toluene phase was collected, dried by rotary evaporation, and rinsed extensively with methanol to obtained purified metal nanoparticles and were denoted as M-EPA (M=Pd, Au).

Characterizations. The morphology and size of the EPA capped metal nanoparticles were characterized by transition electron microscopic (TEM) studies (Philips CM300 at 300 kV). FTIR measurements were carried out with a PerkinElmer FTIR spectrometer (Spectrum One,
spectral resolution 4 cm-1), where the samples were prepared by drop-casting the nanoparticle solution onto a NaCl disk. UV–vis spectra were collected with a PerkinElmer Lambda 35 UV–vis spectrometer, and photoluminescence measurements were performed with a PTI fluorospectrometer.

Results and discussions

The products of these metal nanoparticles capped by EPA were firstly characterized by transition electronic microscopic measurements (TEM) and the results were shown in figure 1. As shown in figure $1A_1$-F_1, the well-dispersed nanoparticles nature without apparent aggregation of nanoparticles is clear, informing that all the metal nanoparticles were well protected by the surface ligands. The lattice spacing of various metals were also predicted by high-resolution TEM which are depicted in figure $1A_2$-F_2, specifically, are d_{100}=0.234 nm (fcc Ru, JCPDS no. 88-2333),[20] d_{111}=0.220 nm (fcc Rh, JCPDS card no. 5-685),[21] d_{111}=0.226 nm (fcc Pd, JCPDS card no. 46-1043),[22] d_{111}=0.225 nm (fcc, Ir, JCPDS card no. 46-1044),[22] d_{111}=0.230 nm (fcc Pt, JCPDS card no. 4-802),[22] and d_{111}=0.235 nm (fcc Au, JCPDS card no. 4-784),[22] suggesting that all the metal nanoparticles are in good agreement with their bulk crystalline structures. While the core size of those metal nanoparticles are slightly different from each other, in detail, are 1.55 ± 0.37 nm, 1.3 ± 0.6 nm, 2.50 ± 0.56 nm, 1.37 ± 0.37 nm, 1.55 ± 0.46 nm and 2.20 ± 0.64 nm for Ru-EPA, Rh-EPA, Pd-EPA, Ir-EPA, Pt-EPA and Au-EPA, respectively (figure $1A_3$-F_3).

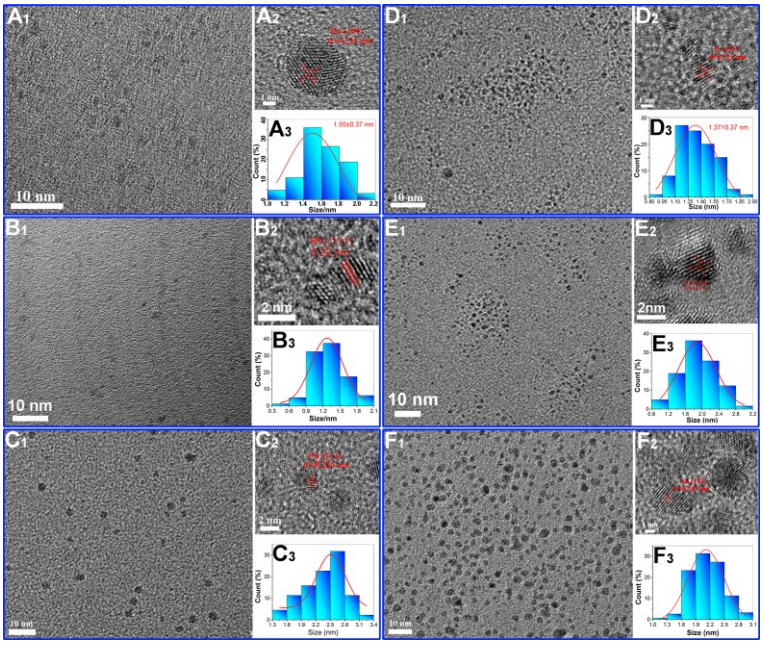

Figure 1. Represent TEM images of various metals (A: Ru, B: Rh, C: Pd, D: Ir, E: Pt, F: Au) functionalized by ethynylphenylacetylene (A_1-F_1) and the corresponding HETEM images with lattice spacing marked (A_2-F_2) and histogram of size distribution (A_3-F_3).

The surface structures of the EPA functionalized metal nanoparticles were studied by FTIR measurements and the full spectra of M-EPA nanoparticles were depicted in figure 2A. As shown, for all the samples, the ≡C-H vibration, of which should present at 3294 cm^{-1} for monomeric EPA, disappeared as expected, indicating that the cleavage of the ≡C-H bonds.[23] And the presence of other vibration peaks such as CH_2 and CH_3 from the ethyl groups in the range of 2800-3000 cm^{-1} informed the EPA ligands were successfully bounded onto the metal nanoparticles' surface. Furthermore, the C≡C vibration of M-EPA red-shifted to lower wavenumbers compared to that of monomeric EPA at 2108 cm^{-1} because of the intraparticle charge delocalization which has been well investigated in our previous study.[10, 12] When zooming in the range around C≡C vibration (figure 2B), it was found that there are more than one peak for some metals, for instance, Ir-EPA has peaks at 2018 and 1965 cm^{-1}, Pt-EPA has peaks at 2033 and 1973 cm^{-1}, Ru-EPA has peaks at 2020 and 1953 cm^{-1} and etc., which make it hard to understand. This can be explained by the formation of metal-acetylide (M-C≡C-), metal-hydride (M-H) and/or metal-vinylidene (M=C=CH-) interfacial bonds which are in a

dynamic equilibrium while their vibrations are very close to each other or even overlapped and hard to distinguished.[10-11, 24] Besides that, there are more difference between the monomeric EPA and M-EPA when the spectra were zoomed in as shown in figure 2C. One may notice that the spectral feature of aromatic ring =C-H vibrational stretch peak for the monomeric EPA is located at 3042 cm^{-1}, while for all the M-EPA nanoparticle, the aromatic ring =C-H vibrational stretch peaks red-shifted to lower wavenumbers, indicating that the bonding order decreased after bounded onto metal nanoparticles than monomer. This can be explained by effective intraparticle charge delocalization through either M-C≡C- or M=C=CH- interfacial bonds. Similar observations of aromatic ring =C-H vibrational stretch red-shift were also witnessed by previous studies such as vinylanthracene functionalized Ru nanoparticles,[25] and ethynylferrocene functionalized Pt nanoparticle and nanoclusters.[26] More interestingly, for the 5d metals, it was found that the aromatic ring =C-H vibrational stretch decreased with the increase of d-electrons, from 3023 cm^{-1} for Ir-EPA, 3021 cm^{-1} for Pt-EPA to 3020 cm^{-1} for Au-EPA. While for 4d metals, the trend is the same as the 5d metals but Pd is an exception. In detail, aromatic ring =C-H vibrational stretch decreased from 3021 cm^{-1} for Ru-EPA to 3019 cm^{-1} for Rh-EPA while it increased to 3022 cm^{-1} for Pd-EPA. This might be accounted for the different degree of intraparticle charge delocalization effected by the number of d-electrons (vide infra).

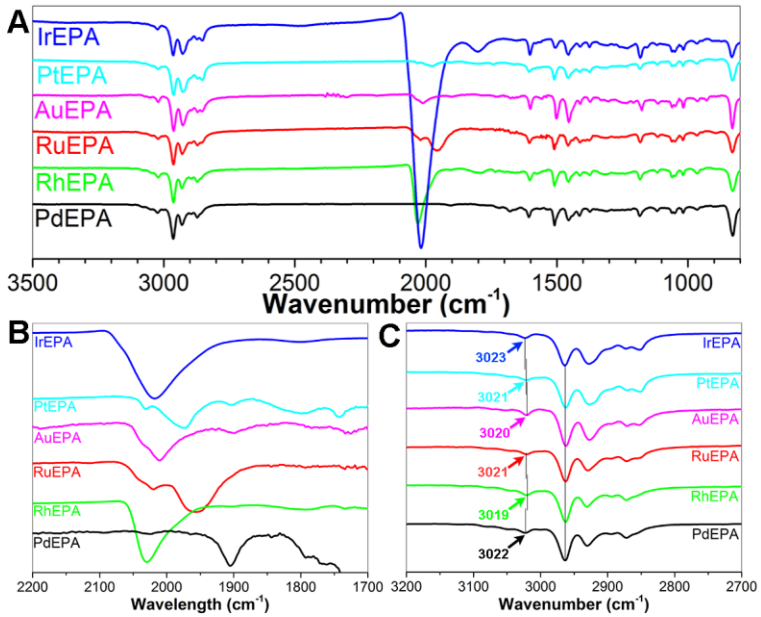

Figure 2. FTIR spectra of various metals (Ir, Pt, Au, Ru, Rh and Pd) capped by EPA (A) and the zooming at the range of -C≡C- vibration (B) and at the range of aromatic ring =C-H vibrational stretch (C).

Based on our prior work,[26-28] now it is well-known that when alkyne bounded onto metal nanoparticle, the resulting products would show unique optical characteristics which can be characterized by UV-vis and fluorescence spectroscopies due to the intraparticle charge delocalization through metal nanoparticles as they behaved analogously to diacetylene (-C≡C-C≡C-) derivatives.[29-30] In this case, these characteristics were also observed as shown in figure 3. First of all, figure 3A depicted the UV-vis absorption spectra of 5d M-EPA nanoparticles and both Ir-EPA and Pt-EPA exhibited decay profiles which are consistent with the Mie characteristics of metal nanoparticle while Au-EPA exhibited a absorption peak at around 510 nm due the well-known surface plasmon resonance.[31-32] At the same time, apparent photoluminescence was observed as except, while the excitation and emission peak positions

were slightly different as shown in figure 3B. For example, the excitations are increased from 334 nm for Ir-EPA, 338 nm for Pt-EPA, to 343 nm for Au-EPA, and the emissions (highlighted by red lines) are also increased from 388 nm, 399 nm, to 403 nm for Ir-EPA, Pt-EPA and Au-EPA, respectively, with the increase of 5d electron. On the other hand, figure 3C-D depicted the UV-vis and photoluminescence spectra of EPA functionalized 4d metals (Ru, Rh and Pd). Similarly to Pt-EPA and Ir-EPA, these three 4d M-EPA nanoparticles exhibited the decay feature of Mie characteristics. As for photoluminescence profiles, the excitation is increased from 381 nm (Ru-EPA) to 390 nm (Rh-EPA) while deceased to 370 nm (Pd-EPA); and the emissions (highlighted by red lines) are 458 nm, 479 nm, 452 nm, which are in the same order as excitation. Compared with 5d metals, it was found that the excitation and emission peak positions are all in the same trend with the increase of d electrons while Pd is an exception (which also happened to aromatic ring =C-H vibrational stretches of the as-prepared M-EPA nanoparticles). In another word, the strength of intraparticle charge delocalization through metal nanoparticles in the same period (Ir, Pt, Au and Ru, Rh, Pd) is decreased with the increase of d-electrons except Pd.

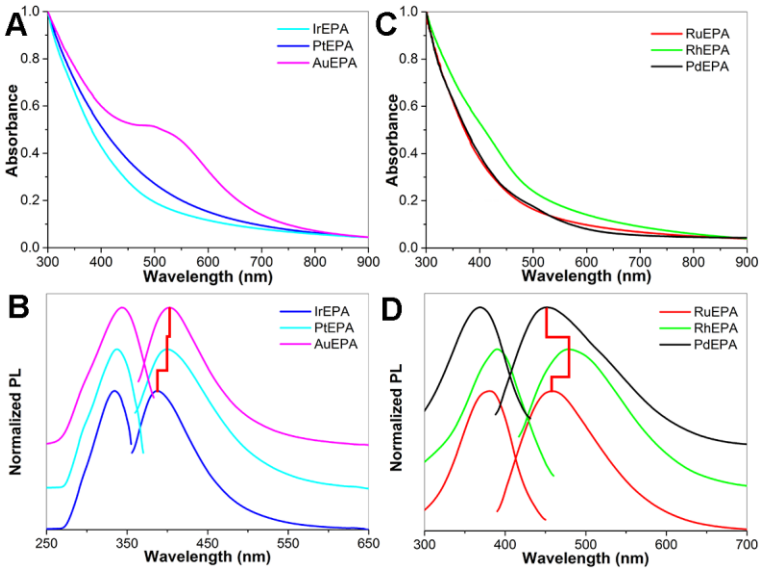

Figure 3. (A-B): UV-vis and PL spectra of 5d metal (Ir, Pt and Au) nanoparticles functionalized by EPA. (C-D): UV-vis and PL spectra of 4d metal (Ru, Rh and Pd) nanoparticles functionalized by EPA.

To explain the spectroscopic trend (including FTIR and PL) caused by the intraparticle charge delocalization, the d-electron effect of the metals is considered. In particular, scheme 1, illustrated the interfacial bonding of M=C=C-, and as shown, the formation of M=C bonding involves a synergistic process with electrons donated from the filled π-orbital or lone-pair electrons of ligands (EPA in this case) into an empty orbitals of metals to form a donor-acceptor bond (σ bond), while with electrons back-donated from the d-orbitals of the metal into the empty π*-orbital of ligands for form a dπ-pπ bond.[33-36] And the intraparticle charge delocalization is highly depended on the strength of the dπ-pπ bond at the interface of metal nanoparticle and organic ligands. However, the electron configurations of metals are different from each other. Based on traditional chemistry, the electron configurations of 5d metals are Ir [Xe-$6s^2 4f^{14} 5d^7$, Pt [Xe-$6s^1 4f^{14} 5d^9$, and Au [Xe-$6s^1 4f^{14} 5d^{10}$. With the increase of the 5d electrons, the empty d-orbitals of metals will decrease, which means the electron acceptors will decrease, as a result,

the strength of the σ bond will be weaken with the increase of 5d electrons. And the dπ-pπ bond is highly depends on the σ bond, briefly, with the weakening of σ bond, the M=C bonding length will decrease and as a results, the overlap of d-electron orbital of metals and π*-orbital of ligands will decrease and this will further weaken the M=C bonding. This is consistent with the PL and FTIR spectroscopic results. Similarly, the electron configurations of 4d metals are Ru [Kr-$5s^1 4d^7$, Rh [Kr-$5s^1 4d^8$, and Pd [Kr-$5s^0 4d^{10}$ and the explaination above is still valid for Ru to Rh but invalid for Rh to Pd as Pd is an exception as mentioned before. To explain this exception, the electron affinity (E_{ea}) of metals is checked and E_{ea} values are 101.1, 109.7 and 54.2 kJ/mol for Ru, Rh and Pd, respectively (E_{ea} values are 151.0, 205.3 and 222.7 kJ/mol for Ir, Pt and Au, respectively), of which E_{ea} of Pd is also and exception in this period.[37] As the dπ-pπ bond is from 4d-electrons back-donation into empty π*-orbital, the back-donation of d-electrons is more difficult when the EA is low. That's why the situation for Pd is an exception.

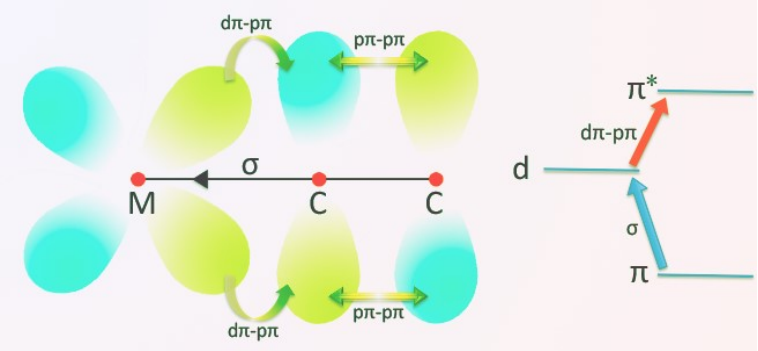

Scheme. Diagram of the interfacial bonding of M=C=C, M=Ir, Pt, Au, and Ru, Rh, Pd.

Conclusion

Acknowledgement

blablabla

References

Primary Sources

Secondary Sources

Uncategorized References

1. Murray, R. W., Nanoelectrochemistry: Metal nanoparticles, nanoelectrodes, and nanopores. *Chem Rev* **2008,** *108* (7), 2688-2720.
2. Hopkinson, M. N.; Richter, C.; Schedler, M.; Glorius, F., An overview of N-heterocyclic carbenes. *Nature* **2014,** *510* (7506), 485-496.
3. Tamura, M.; Fujihara, H., Chiral bisphosphine BINAP-stabilized gold and palladium nanoparticles with small size and their palladium nanoparticle-catalyzed asymmetric reaction. *J Am Chem Soc* **2003,** *125* (51), 15742-15743.

4. Daniel, M. C.; Astruc, D., Gold nanoparticles: Assembly, supramolecular chemistry, quantum-size-related properties, and applications toward biology, catalysis, and nanotechnology. *Chem Rev* **2004,** *104* (1), 293-346.
5. Hu, P. G.; Chen, L. M.; Kang, X. W.; Chen, S. W., Surface Functionalization of Metal Nanoparticles by Conjugated Metal-Ligand Interfacial Bonds: Impacts on Intraparticle Charge Transfer. *Accounts Chem Res* **2016,** *49* (10), 2251-2260.
6. Kang, X. W.; Song, Y.; Chen, S. W., Nitrene-functionalized ruthenium nanoparticles. *J Mater Chem* **2012,** *22* (36), 19250-19257.
7. Chen, L. M.; Hu, P. G.; Deming, C. P.; Li, W.; Li, L. G.; Chen, S. W., Chemical Reactivity of Naphthalenecarboxylate-Protected Ruthenium Nanoparticles: Intraparticle Charge Delocalization Derived from Interfacial Decarboxylation. *J Phys Chem C* **2015,** *119* (27), 15449-15454.
8. Chen, L. M.; Song, Y.; Hu, P. G.; Deming, C. P.; Guo, Y.; Chen, S. W., Interfacial reactivity of ruthenium nanoparticles protected by ferrocenecarboxylates. *Phys Chem Chem Phys* **2014,** *16* (35), 18736-18742.
9. Deming, C. P.; Kang, X. W.; Liu, K.; Chen, S. W., Nitrene-functionalized ruthenium nanoparticles: Selective manipulation of nanoparticle electronic conductivity by vinyl derivatives. *Sensor Actuat B-Chem* **2014,** *194*, 319-324.
10. Kang, X. W.; Zuckerman, N. B.; Konopelski, J. P.; Chen, S. W., Alkyne-Functionalized Ruthenium Nanoparticles: Ruthenium-Vinylidene Bonds at the Metal-Ligand Interface. *J Am Chem Soc* **2012,** *134* (3), 1412-1415.
11. Hu, P. G.; Chen, L. M.; Deming, C. P.; Bonny, L. W.; Lee, H. W.; Chen, S. W., Identification of the formation of metal-vinylidene interfacial bonds of alkyne-capped platinum nanoparticles by isotopic labeling. *Chem Commun* **2016,** *52* (78), 11631-11633.
12. Kang, X. W.; Zuckerman, N. B.; Konopelski, J. P.; Chen, S. W., Alkyne-Stabilized Ruthenium Nanoparticles: Manipulation of Intraparticle Charge Delocalization by Nanoparticle Charge States. *Angew Chem Int Edit* **2010,** *49* (49), 9496-9499.
13. Hu, P. G.; Chen, L. M.; Deming, C. P.; Kang, X. W.; Chen, S. W., Nanoparticle-Mediated Intervalence Charge Transfer: Core-Size Effects. *Angew Chem Int Edit* **2016,** *55* (4), 1455-1459.
14. Deming, C. P.; Zhao, A.; Song, Y.; Liu, K.; Khan, M. M.; Yates, V. M.; Chen, S. W., Alkyne-Protected AuPd Alloy Nanoparticles for Electrocatalytic Reduction of Oxygen. *Chemelectrochem* **2015,** *2* (11), 1719-1727.
15. He, G. Q.; Song, Y.; Kang, X. W.; Chen, S. W., Alkyne-functionalized palladium nanoparticles: Synthesis, characterization, and electrocatalytic activity in ethylene glycol oxidation. *Electrochim Acta* **2013,** *94*, 98-103.
16. Liu, K.; Song, Y.; Chen, S. W., Electrocatalytic activities of alkyne-functionalized copper nanoparticles in oxygen reduction in alkaline media. *J Power Sources* **2014,** *268*, 469-475.
17. Chen, W.; Chen, S. W.; Ding, F. Z.; Wang, H. B.; Brown, L. E.; Konopelski, J. P., Nanoparticle-mediated intervalence transfer. *J Am Chem Soc* **2008,** *130* (36), 12156-12162.
18. Hu, P. G.; Duchesne, P. N.; Song, Y.; Zhang, P.; Chen, S. W., Self-Assembly and Chemical Reactivity of Alkenes on Platinum Nanoparticles. *Langmuir* **2015,** *31* (1), 522-528.
19. Hu, P. G.; Song, Y.; Chen, L. M.; Chen, S. W., Electrocatalytic activity of alkyne-functionalized AgAu alloy nanoparticles for oxygen reduction in alkaline media. *Nanoscale* **2015,** *7* (21), 9627-9636.
20. Ye, H. H.; Wang, Q. X.; Catalano, M.; Lu, N.; Vermeylen, J.; Kim, M. J.; Liu, Y. Z.; Sun, Y. G.; Xia, X. H., Ru Nanoframes with an fcc Structure and Enhanced Catalytic Properties. *Nano Lett* **2016,** *16* (4), 2812-2817.
21. Biacchi, A. J.; Schaak, R. E., The Solvent Matters: Kinetic versus Thermodynamic Shape Control in the Polyol Synthesis of Rhodium Nanoparticles. *Acs Nano* **2011,** *5* (10), 8089-8099.
22. Wang, X.; Zhuang, J.; Peng, Q.; Li, Y. D., A general strategy for nanocrystal synthesis. *Nature* **2005,** *437* (7055), 121-124.
23. Liu, K.; Kang, X. W.; Zhou, Z. Y.; Song, Y.; Lee, L. J.; Tian, D.; Chen, S. W., Platinum nanoparticles functionalized with acetylene derivatives: Electronic conductivity and electrocatalytic activity in oxygen reduction. *J Electroanal Chem* **2013,** *688*, 143-150.
24. Bianchini, C.; Peruzzini, M.; Vacca, A.; Zanobini, F., Metal Hydride Alkynyl -] Metal Vinylidene Rearrangements Occurring in Both Solid-State and Solution - Role of the 1-Alkyne Substituent in Determining the Relative Stability of Pi-Alkyne, Hydride Alkynyl, and Vinylidene Forms at Cobalt. *Organometallics* **1991,** *10* (10), 3697-3707.

25. Chen, W.; Pradhan, S.; Chen, S., Photoluminescence and conductivity studies of anthracene-functionalized ruthenium nanoparticles. *Nanoscale* **2011,** *3* (5), 2294-300.
26. Hu, P.; Chen, L.; Deming, C. P.; Kang, X.; Chen, S., Nanoparticle-Mediated Intervalence Charge Transfer: Core-Size Effects. *Angewandte Chemie* **2016,** *55* (4), 1455-9.
27. Hu, P. G.; Chen, L. M.; Deming, C. P.; Lu, J. E.; Bonny, L. W.; Chen, S. W., Effects of para-substituents of styrene derivatives on their chemical reactivity on platinum nanoparticle surfaces. *Nanoscale* **2016,** *8* (23), 12013-12021.
28. Chen, W.; Zuckerman, N. B.; Kang, X. W.; Ghosh, D.; Konopelski, J. P.; Chen, S. W., Alkyne-Protected Ruthenium Nanoparticles. *J Phys Chem C* **2010,** *114* (42), 18146-18152.
29. Black, H. K.; Horn, D. H. S.; Weedon, B. C. L., Studies with Acetylenes .1. Some Reactions of Grignard Reagents with Alk-1-Ynyl and Alk-1-Enyl Halides. *J Chem Soc* **1954,** (Jun), 1704-1709.
30. Warta, R.; Sixl, H., Optical-Absorption and Fluorescence Spectroscopy of Stable Diacetylene Oligomer Molecules. *J Chem Phys* **1988,** *88* (1), 95-99.
31. Mie, G., Articles on the optical characteristics of turbid tubes, especially colloidal metal solutions. *Ann Phys-Berlin* **1908,** *25* (3), 377-445.
32. Eustis, S.; El-Sayed, M. A., Why gold nanoparticles are more precious than pretty gold: Noble metal surface plasmon resonance and its enhancement of the radiative and nonradiative properties of nanocrystals of different shapes. *Chem Soc Rev* **2006,** *35* (3), 209-217.
33. Wakatsuki, Y.; Koga, N.; Yamazaki, H.; Morokuma, K., Acetylene Pi-Coordination, Slippage to Sigma-Coordination, and 1,2-Hydrogen Migration Taking Place on a Transition-Metal - the Case of a Ru(Ii) Complex as Studied by Experiment and Ab-Initio Molecular-Orbital Simulations. *J Am Chem Soc* **1994,** *116* (18), 8105-8111.
34. Slugovc, C.; Sapunov, V. N.; Wiede, P.; Mereiter, K.; Schmid, R.; Kirchner, K., Ruthenium(II) tris(pyrazolyl)borate complexes. Reversible vinylidene complex formation. *J Chem Soc Dalton* **1997,** (22), 4209-4216.
35. Wakatsuki, Y., Mechanistic aspects regarding the formation of metal vinylidenes from alkynes and related reactions. *J Organomet Chem* **2004,** *689* (24), 4092-4109.
36. Braunschweig, H.; Ye, Q.; Vargas, A.; Dewhurst, R. D.; Radacki, K.; Damme, A., Controlled homocatenation of boron on a transition metal. *Nat Chem* **2012,** *4* (7), 563-567.
37. Dean, J. A., *Lange's Handbook of Chemistry*. 15th ed.; McGraw-Hill Professional: United States of America, 1998.